INTERNATIONAL ATOMIC ENERGY AGENCY
UNITED NATIONS EDUCATIONAL, SCIENTIFIC AND CULTURAL ORGANIZATION

INTERNATIONAL CENTRE FOR THEORETICAL PHYSICS
34100 TRIESTE (ITALY) - P.O.B. 586 - MIRAMARE - STRADA COSTIERA 11 - TELEPHONE: 2240-1
CABLE: CENTRATOM - TELEX 460392 - I

H4.SMR 346/ 12

SCHOOL ON
NON-ACCELERATOR PHYSICS
25 April - 6 May 1988

EXTENSIVE AIR SHOWER ARRAYS

by

G. Navarra
Istituto di Cosmogeofisica del CNR
Torino

CERENKOV COUNTERS

L. Koch-Miramond. Proc. 17th ICRC, 12, 21 (1981)

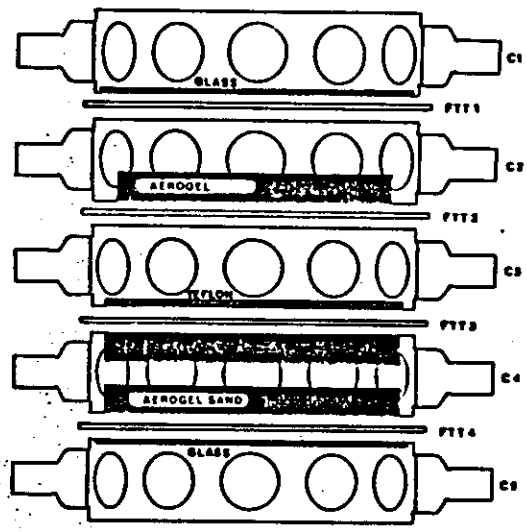

Fig. 1. The HEAO-3 C2 detector configuration. C1 to C5 Cerenkov counters with refractive indices: $n_1 = n_5 = 1.64$; $n_2 = 1.033$; $n_3 = 1.33$; $n_4 = 1.012$ and diameters around 60 cm. PTT 1 to 4 flash tube hodoscope with four trays, each of which contains two layers of 128 flash tubes. Time of flight system between C1 and C5 counters.

GRIGOROV et al Proc Hobart Conf, 5 (1971) 1746

CALORIMETERS

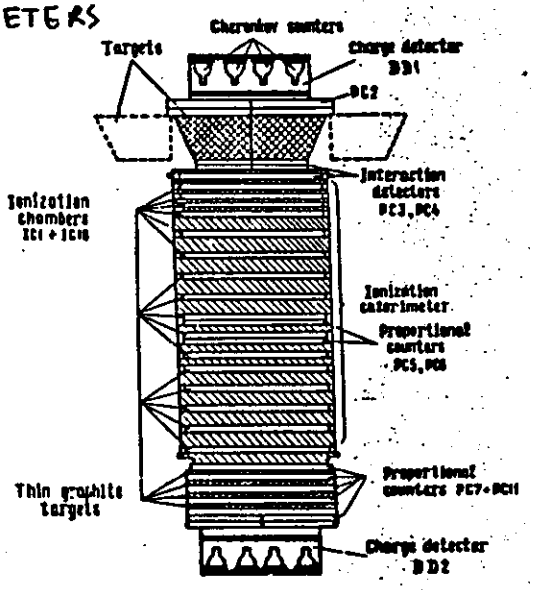

clear cascade process. The detectors on the top,

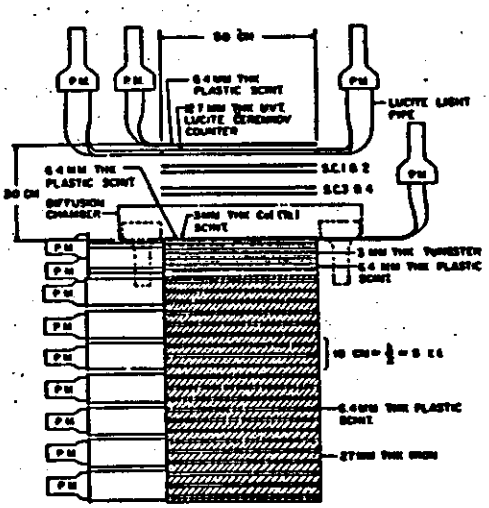

FIG. 1. Balloon-borne ionization spectrometer. SC_1, SC_2, SC_3, and SC_4 are wire-grid spark chambers with core readout to determine the trajectory of the incident particle and to help in rejecting background events. The detector system was designed so that a very wide range of charges and energies could be measured with a single instrument.

RYAN et al PRL 28 985 (1972)

JAPANESE-AMERICAN COOPERATIVE EMULSION EXPERIMENT (JACEE)

R. W. Huggett, S. D. Hunter, W. V. Jones, and Y. Takahashi
Department of Physics and Astronomy
Louisiana State University
Baton Rouge, LA 70803 USA

T. Ogata and T. Saito, ICR, University of Tokyo, JAPAN
R. Holynski, A Jurak, W. Wolter, and B. Wosiek, INP, Krakow, POLAND
S. Dake, M. Fuki, and T. Tominaga, Kobe University, JAPAN
R. M. Friedlander and H. H. Heckman, Lawrence Berkeley Laboratory, USA
T. A. Parnell, NASA Marshall Space Flight Center, USA
O. Miyamura, Osaka University, JAPAN
J. C. Gregory, University of Alabama, Huntsville, USA
T. H. Burnett, J.J. Lord, and R. J. Wilkes, University of Washington, USA
T. Hayashi, J. Iwai, and T. Tabuki, Waseda University, JAPAN

ABSTRACT

Balloon flights are being used to
charge composition, and energy spectra
energies from 2 TeV to more than 100
factor is achieved with a thin, large
ater. Etchable plastics are used in
for charge measurements. The energy
scanning x-ray films interspersed in
flight in September 1981 will employ
vide direct inflight calibration of t

1. Introduction

A collaboration between groups in Jap
lished for the purpose of studying cosmic
heavy nuclei up to 1 TeV/nucleon and prot
jectives involve studies of nucleus-nucle
actions, searches for new particles/phenos
cosmic ray astrophysics. The observation
extensive air showers (EAS) because of th
energies. Data on the ratio of light (Li
medium (C + O) source nuclei at TeV/nucle
between the currently popular models of c
nested leaky box, and closed galaxy model
Fe, C + O, and protons will help in deter
composition is energy dependent.

Several long-duration balloon flights
objectives. The basic detector has a geo
2.5 m^2 sr. It must be exposed for more t
3-4 g/cm^2. Three flights have been compl
engineering flight of a one-quarter area
Sanriku Balloon Center in Japan in May 19
launched from Palestine, Texas; one for 2
for 30 hr in October 1980. These three f
of about 120 m^2 sr hr.

The next flight is planned for Septem
employ electronic counters (gas Cerenkov,
different refractive indices, proportional

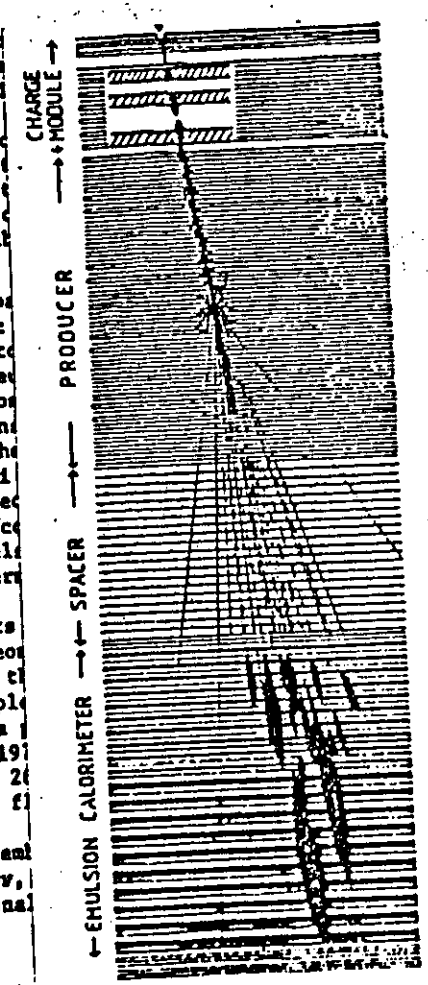

plastic scintillator) in addition to the basic emulsion calorimeter. Although this hybrid apparatus will have a greatly reduced geometrical factor (0.2 m^2 sr) it will provide direct inflight calibration of the passive detectors used in the previous flights. It will also permit studies at energies greater than 20 GeV/nucleon of nucleus-nucleus interactions of particles having independently known charges and energies.

2. Apparatus

The basic passive detector is what has been known as an emulsion chamber. It consists of doubly-coated nuclear emulsions on 800 micron thick methacryl substrates, x-ray films, etchable (CR-39) detectors, low density spacers, and lead sheets (1.0 and 2.5 cm thick). The instrument is segmented into (1) a primary charge module, (2) a target section, (3) a spacer section, and (4) a lead-emulsion calorimeter. This design satisfies three notable requirements for the proposed experiment: (1) accurate charge determinations for the primary nuclei with charge resolution practically independent of energy, (2) reliable energy determinations with energy resolution essentially independent of energy, and (3) a large geometrical factor for collecting the high energy events while rejecting the low energy background. The following table give the salient features of the detector.

SALIENT FEATURES OF THE PASSIVE DETECTION SYSTEM

Weight: 580 kg
Dimensions: 80 cm x 100 cm x 36.6 cm
Geometric factor: 2.5 m^2 sr
Energy thresholds: $E \geq 300$ GeV/nucleon: Electromagnetic cascades visible to naked eye in x-ray film
$E \geq 20$ GeV/nucleon: Observation of α-jets within spacer section
Target: methacryl (lucite): 0.2 nuclear interaction length for protons
0.8 nuclear interaction length for Fe
Energy resolution: $\Delta E/E$
1) γ-ray cascades: 20%
2) Primary nucleus: < 50%
Charge resolution: $\Delta Z/Z$ - 1 for Fe, < 1 for smaller Z
Track sensitive detectors: 1) Fuji nuclear emulsions, types 7B and 6B
2) Sakura N-type x-ray film
3) Etchable plastic CR-39

This basic detector was flown in the engineering flight and in the first two full-scale flights, but only the first full-scale flight employed the spacer section. Acoustic detection of the highest energy events was tested in the 1980 flight by using silicone grease to bond PZ disk transducers to the four edges of the lead plates in the calorimeter. A scintillator placed beneath the calorimeter provided a prompt trigger for the acoustic detectors, as well as burst-energy information.

The hybrid counter-emulsion system to be flown in 1981 is shown schematically in the figure. The gas Cerenkov counter (1) will provide differential energy measurements over the range 20 - 60 GeV/nucleon with energy resolution about 10% for all nuclei from C to Fe. The proportional counter hodoscope (3) has 5 mm wire spacing. A total of 8 planes will be in two sets of two x,y pairs. Particle trajectories will be measured to within 1° for vertical incidence and to within about 1.5° at the maximum angle set by the trigger counter. For a worst-case resolution

A, Astrophys
148, 12 (1985) 17

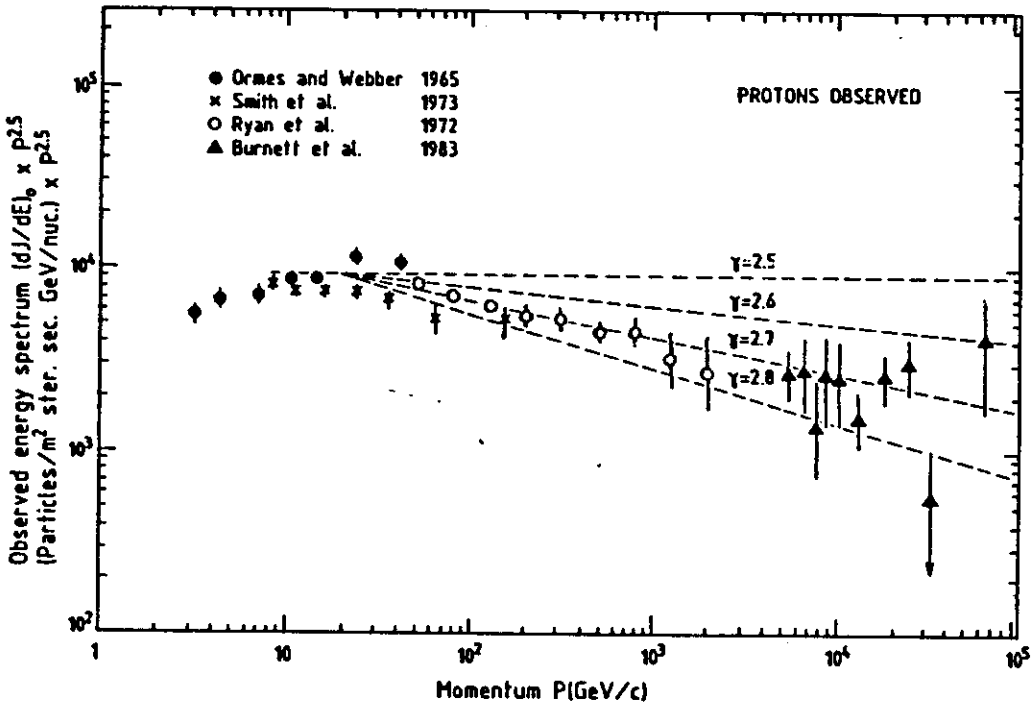

$$\frac{dN}{dE} = A E^{-\gamma}$$

Fig. 10. Energy spectrum of protons observed near Earth as a function of momentum; see legend of Fig. 9

intermediate energies. Above 5 GeV/n the spectra [illegible] well fitted by a single power law with index 2.1 from a few GeV/c/n

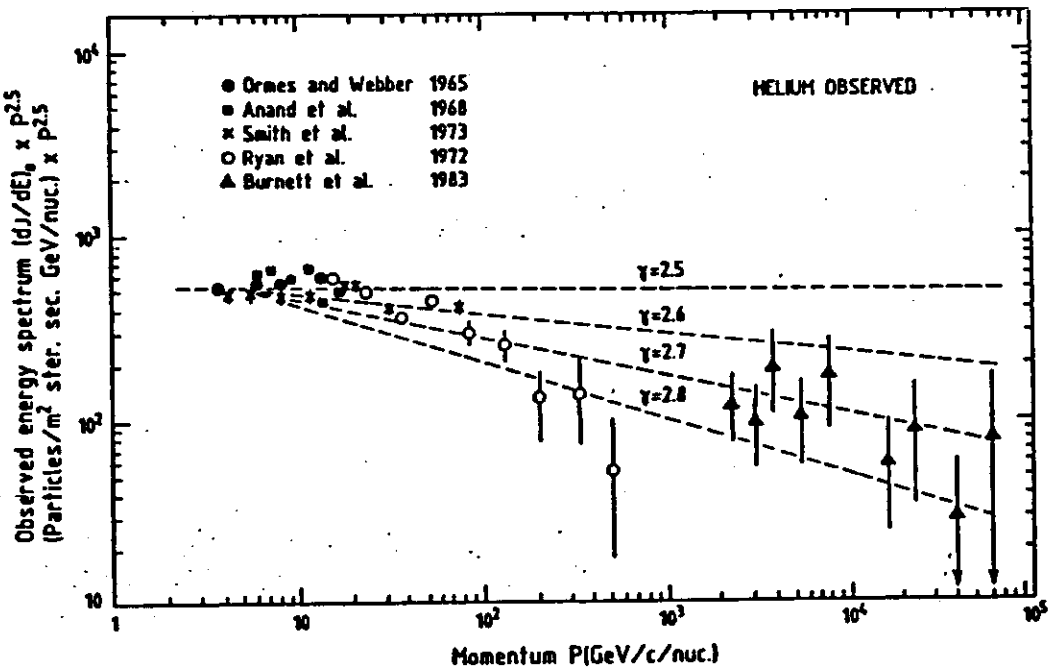

Fig. 11. Energy spectrum of He nuclei observed near Earth as a function of momentum; see legend of Fig. 9

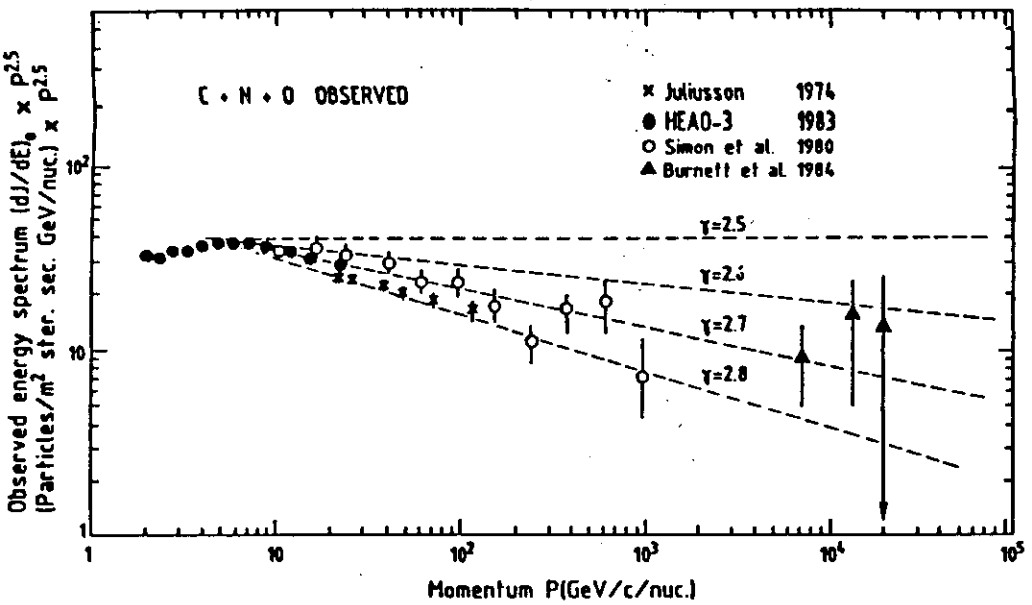

Fig. 9. Energy spectrum of CNO nuclei observed near Earth as a function of momentum P. The spectrum has been flattened by multiplication of the differential flux by $P^{2.5}$. The JACEE integral flux measured above an energy E_0 has been plotted at the energy E_0 and converted into differential flux by multiplication by $1.7/E_0$ where we ve assumed that the index of the integral spectrum is 1.7. Note also that the error bar corresponding to each point does not include the error on the energy etermination of the particle

$\gamma_{source} \simeq \gamma_{det} - 0.4$

Composition and Origin of CR (1983) p 83

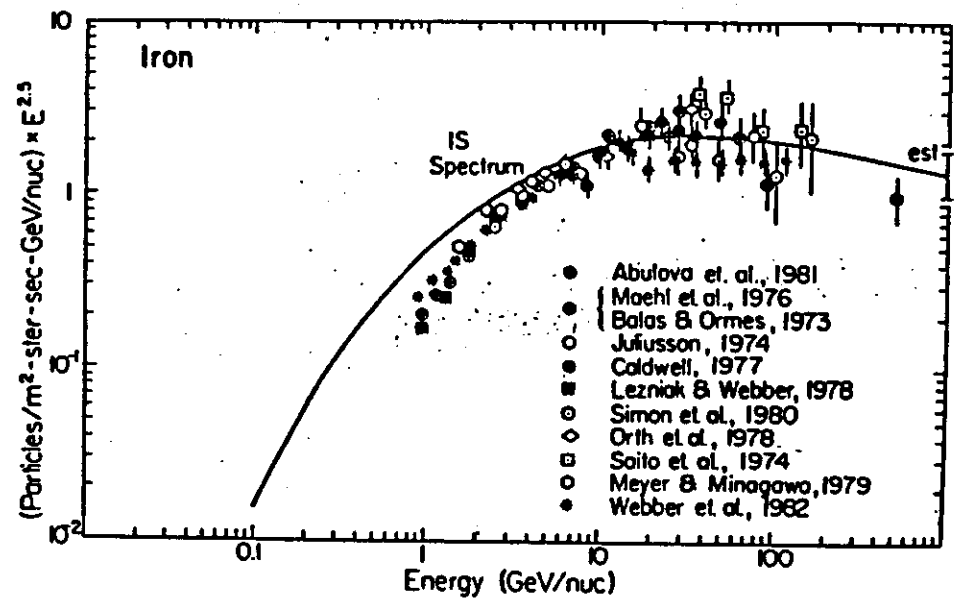

Figure 3. Measurements of Fe nuclei intensities above 1 GeV/nuc. All intensities x $E^{2.5}$.

Significant differences exist in these spectra. The He spectrum appears to reach a peak at ∿ 10 GeV/nuc corresponding to a $E^{-2.5}$ spectrum and then approaches a spectral index ∿ -2.7 at high energies. This high energy spectral index is identical to that for protons. The spectra for O and Fe reach their maxima, corresponding to a $E^{-2.5}$ spectrum, at higher energies, perhaps as high as 50 GeV/nuc for Fe, and the spectral slope appears to continue to increase at higher energies, possibly becoming ∿ -2.7 but but it is difficult to verify this because of lack of measurements

JACEE

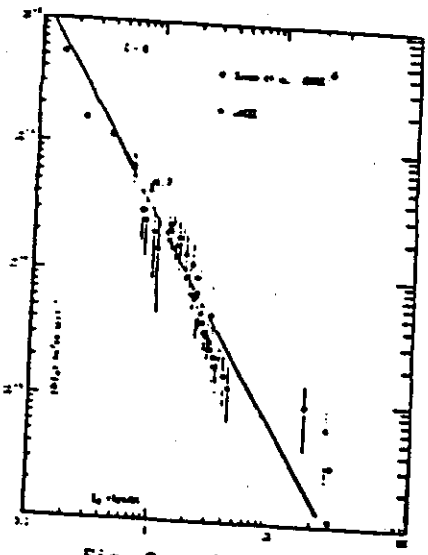

Fig. 2a. (C-O) group.

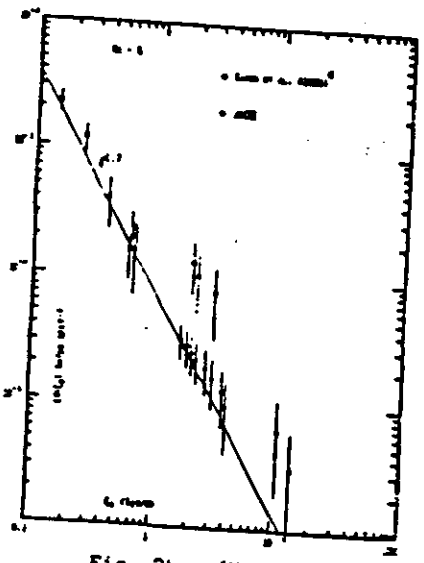

Fig. 2b. (Ne-S) group.

data. For E_o > 100 TeV/nucleus we recorded only one iron primary, whereas 7 iron nuclei are expected if the assumed differential spectral index is -2.4. We may observe a slight enhancement in the fluxes at energies above 10^{14} eV/nucleus, but the statistical significance of the data at the highest energies is insufficient for any firm conclusion. Data currently being analyzed from the recent JACEE 6 flight will increase the statistics of our dataset.

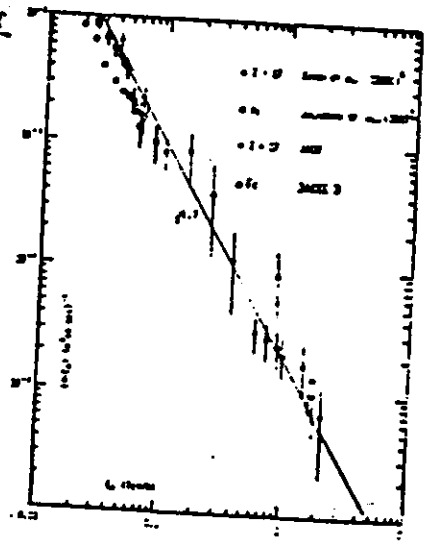

Fig. 2c. (Z≥17) group.

Fig. 2. Integral energy spectra for heavy cosmic ray components.

4. Nucleus-nucleus Interactions

Quantum chromodynamics predicts that at high nuclear temperature and/or high nuclear density the transition to the chirally symmetric phase of matter consisting of deconfined quarks and gluons should occur[11]. It is expected, that such conditions may be created in the collisions of heavy nuclei at high energies, and these prospects stimulated our efforts in detailed study of nucleus-nucleus interactions. The analysis of nuclear collisions recorded in JACEE emulsion chambers resulted in a variety of observations[12]. We present here the results of the inclusive and semi-inclusive analysis followed by the outcome

Low Energy Composition of Primary Cosmic Rays

(from S. Hayakawa, 1979)

Component	Z	Relative intensity for fixed en/nucleon	en/nucleus		
Protons	1	100	100	40.7	
Helium	2	5	52.8	21.5	
Light nuclei	3-5	0.09	3.1	1.3	
Medium Nuclei	6-9	0.33	33	13.4	
Heavy Nuclei	10-19	0.11	31.7	12.9	0.16
Very Heavy Nuclei	>20	0.03	24.8	10.1	.04

4.5 GeV ~ 200 GeV

$$\langle A \rangle = \frac{\Sigma_i w_i A_i^2}{\Sigma_i w_i A_i}$$

3.5 ÷ 4.0 4.5 ÷ 5

E = energy / nucleon $\quad E = \frac{W}{A}$

W = energy / nucleus

$$s(E)dE = k E^{-\gamma} dE$$

$$S(W)dW = k \left(\frac{W}{A}\right)^{-\gamma} \frac{dW}{A} = k A^{\gamma-1} W^{-\gamma} dW$$

EXTENSIVE AIR SHOWERS

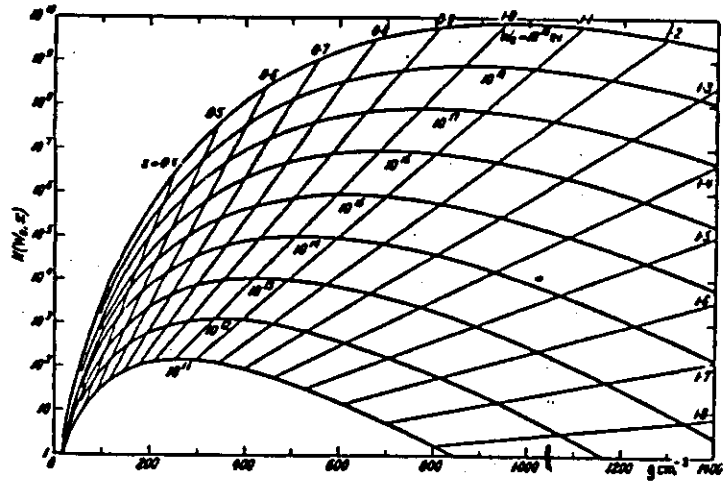

ATM. DEPTH

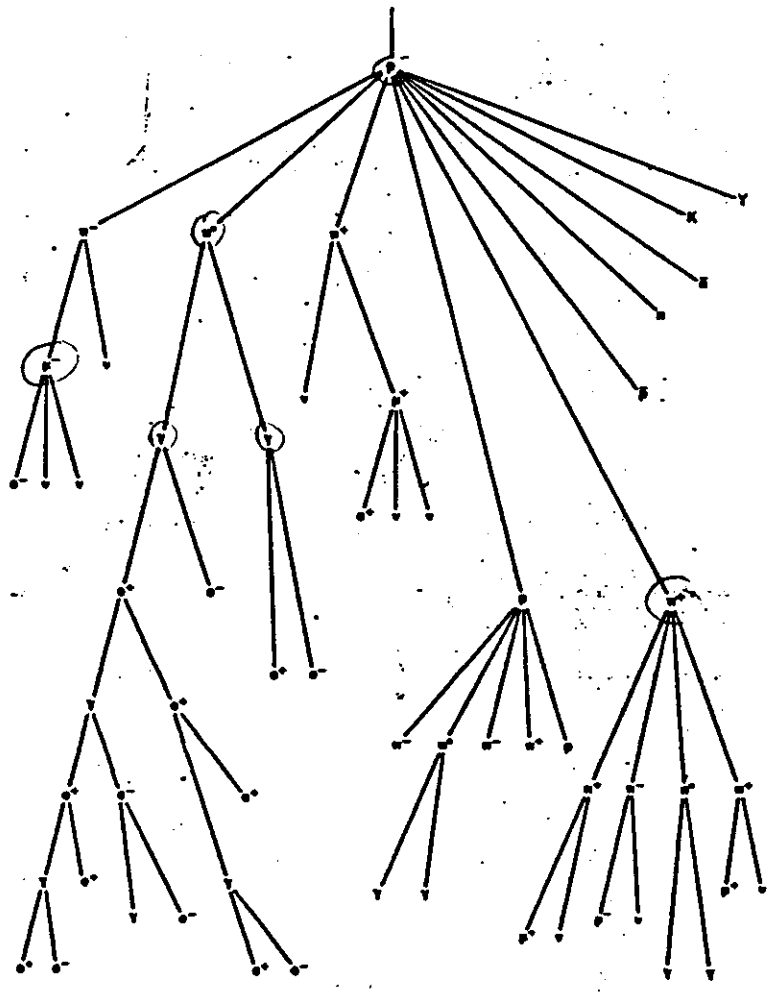

$$b_d^{\pi^\pm} = \frac{h_d}{h_d + h_i} \sim \frac{1}{1 + \frac{E}{120\,\mathrm{GeV}}}$$

can be be represented by the equation[1]

$$N(W_0', t) = \frac{0.31}{\beta_0^{\frac{1}{2}}} \exp\left[t\left(1 - \frac{3}{2}\log s\right)\right] \tag{4.1}$$

where $t = \frac{x}{x_0}$ is the thickness of air in radiation units, $\beta_0 = \log \frac{W_0'}{\varepsilon_0}$, and $s = \frac{3t}{t + 2\beta_0}$.

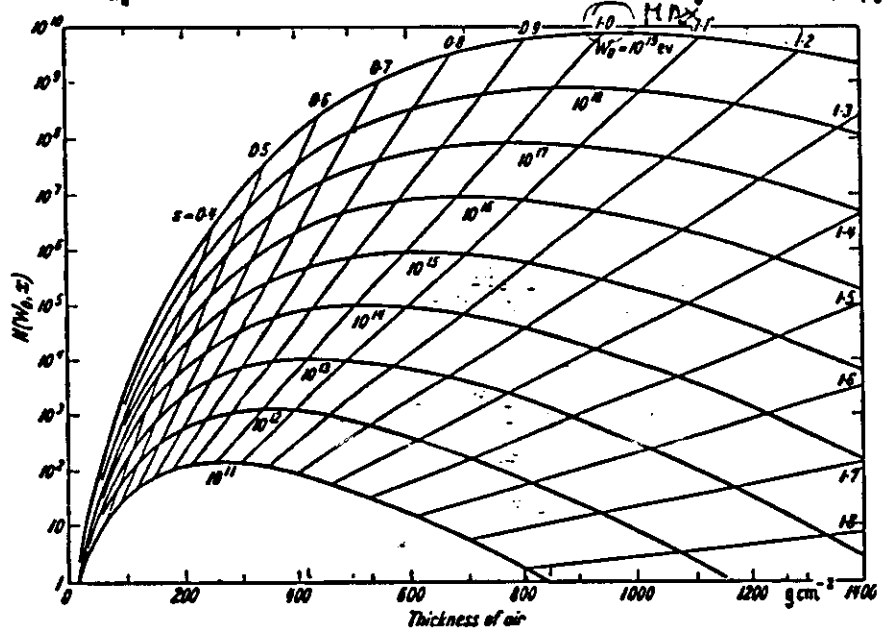

Fig. 1. The total number of electrons, as a function of the thickness (g cm^{-2}) of air crossed, produced by photons of various energies, W_0', in ev. The parameter s is the age of the shower at different stages of its development.

For $E > \varepsilon_0$, the integral energy spectrum of all the electrons in the shower is given by the expression

$$N(W_0', E, t) = \frac{0.135}{\beta^{\frac{1}{2}}} \exp\left[t\left(1 - \frac{3}{2}\log s\right)\right] \tag{4.2}$$

where

$$\beta = \log \frac{W_0}{E} \quad \text{and} \quad s = \frac{3t}{t + 2\beta}.$$

Exact handling of the electrons and photons below the critical energy allows the determination of the integral spectrum for energies $E < \varepsilon_0$ (RICHARDS and NORDHEIM)[2].

In Fig. 2 we have plotted the spectrum in the neighborhood of the maximum development of the shower.

The parameter s is known as the "age" parameter and is simply related to most of the characteristic properties of the shower: its behavior is plotted in Fig. 1. For instance, from Eq. (4.1) it follows that the maximum development of the shower is reached when $s = 1$, i.e., at the thickness

$$t_{max} = \beta_0 = \log \frac{W_0'}{\varepsilon_0}. \tag{4.3}$$

[1] K. GREISEN: Progress in Cosmic Ray Physics, Vol. III, Amsterdam: North Holland Publishing Co. 1956.

[2] J. A. RICHARDS and L. W. NORDHEIM: Phys. Rev. 74, 1106 (1948).

where $E_s = 21.2$ Mev. The natural unit of length of lateral displacement in air is thus

$$r_1 = \frac{E_s}{\varepsilon_0} x_0 = 9.50 \text{ g cm}^{-2} = \frac{73.5}{P} \frac{T}{273} \text{ m} \qquad (5.1)$$

(P in atmosphere and T in °K).

Referring to MOLIÈRE's article for an analysis of the methods of solution, here we give only the results of the calculations performed by NISHIMURA and KAMATA[1], that probably are the most extended and accurate thus far. These results can be considered as reliable as those obtained for the longitutdinal development under approximation B. In Fig. 3 the distribution function $f(r/r_1)$ for all electrons of energy $E \geqq 0$ and for an *homogeneous* atmosphere is plotted for several values of the age parameter, s [2].

The following expression, given by GREISEN[3], represents quite well the results of NISHIMURA and KAMATA for $0.6 \leqq s \leqq 1.8$ and $0.01 \leqq \frac{r}{r_1} \leqq 10$;

$$f\left(\frac{r}{r_1}\right) = C(s)\left(\frac{r}{r_1}\right)^{s-2}\left(\frac{r}{r_1}+1\right)^{s-4.5}. \qquad (5.2)$$

where $C(s)$ assumes the following values:

s	0.6	0.8	1.0	1.2	1.4	1.6	1.8
$C(s)$	0.22	0.31	0.40	0.44	0.43	0.36	0.25

Since the distribution does not depend strongly on s and since the s of showers observed under the same thickness of matter changes slowly as a function of the primary energy W_0', it is justified to assume, in first approximation, that all the showers within a not too great energy range, observed, e.g., at sea level, have the same radial distribution of electrons around the core. This conclusion is convenient for the interpretation of many experimental results.

The curves of Fig. 3 have been evaluated for an homogeneous atmosphere and could be considered valid for the real atmosphere if the equilibrium between the shower and the medium were very good. In this case the variation of the atmospheric pressure, when considering experiments done at different altitudes above sea level, would change only the geometrical length of r_1 and showers of the same age would cover areas proportional to P^{-2}. Actually the equilibrium with the medium is not perfect and the lateral distribution at a certain level is influenced by that at higher levels, where the pressure is smaller. An evaluation of this effect has led GREISEN[3] to formulate the rule that in the lower atmosphere the lateral spread is equal to that observed in a uniform atmosphere having the pressure P_2 of the level two radiation units higher i.e.

$$P_2 = (P - 0.07) \text{ atm.}$$

[1] J. NISHIMURA and K. KAMATA: Prog;. Theo;. Phys. 7, 185 (1952). — KAMATA and NISHIMURA [Suppl. Progr. Theor. Phys. 6, 93 (1958)] give a three-parameter expression that fits their curves somewhat better than that given below (5.2).

[2] Actually the age parameter s as defined by NISHIMURA and KAMATA differs slightly from that of Eq. (4.1). Here $s = \frac{3t}{t + 2\beta_0 + 2\log(r/r_1)}$, and is a slowly varying function of r/r_1 that coincides with our s only for $r/r_1 = 1$. In the lower atmosphere ($t \approx 25$, $\beta_0 \approx 15$) s changes by about 15% when r/r_1 changes by a factor of 10.

[3] K. GREISEN: Progress in Cosmic Ray Physics, Vol. III, Amsterdam: North Holland Publishing 1956.

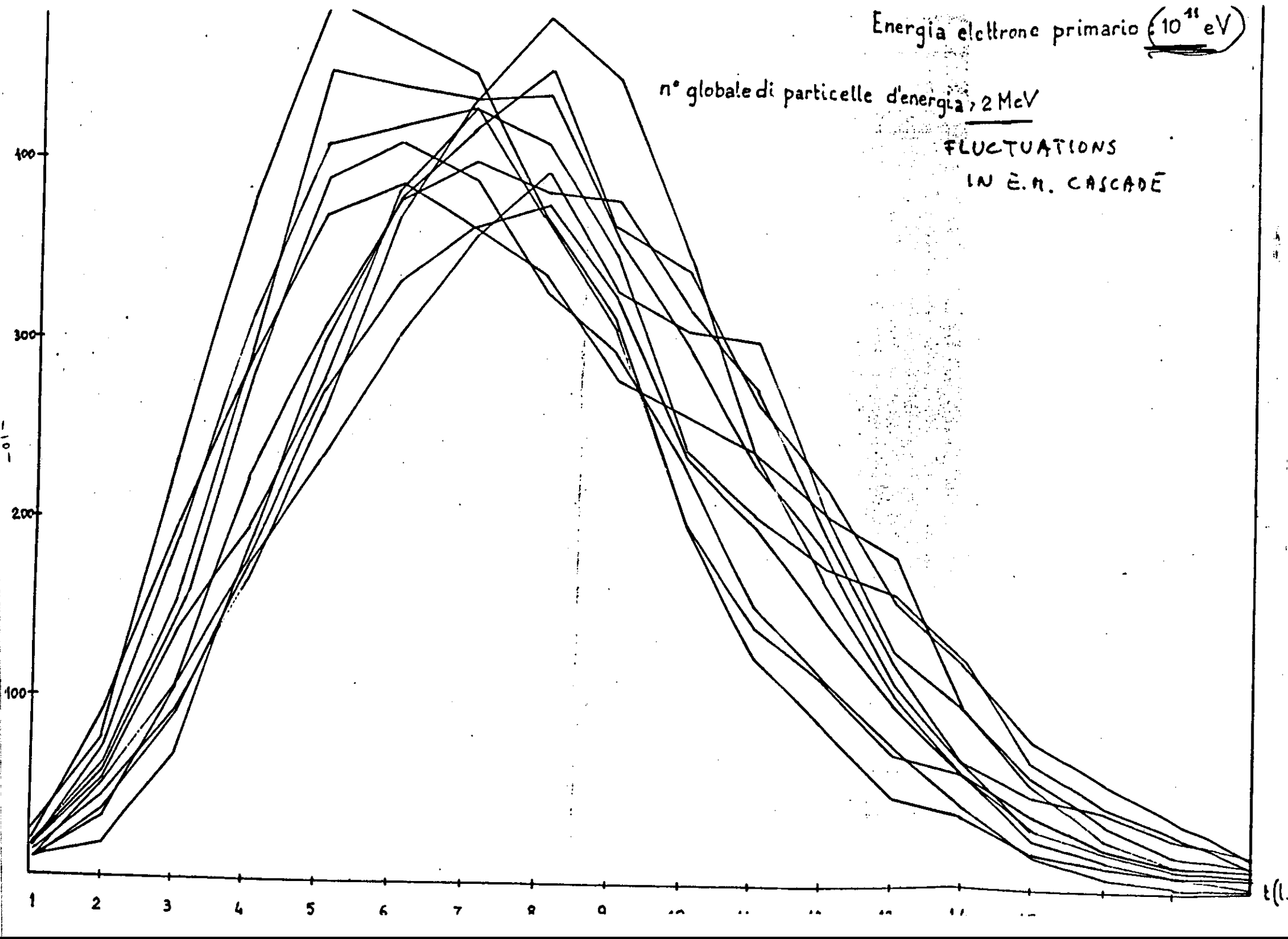
Energia elettrone primario 10^{11} eV
n° globale di particelle d'energia > 2 MeV
FLUCTUATIONS
IN E.M. CASCADE
100
300
200
100
1
2
3
4
5
6
7
8
9

FLUCTUATIONS

→ MEASUREMENTS AT FIXED DEPTH

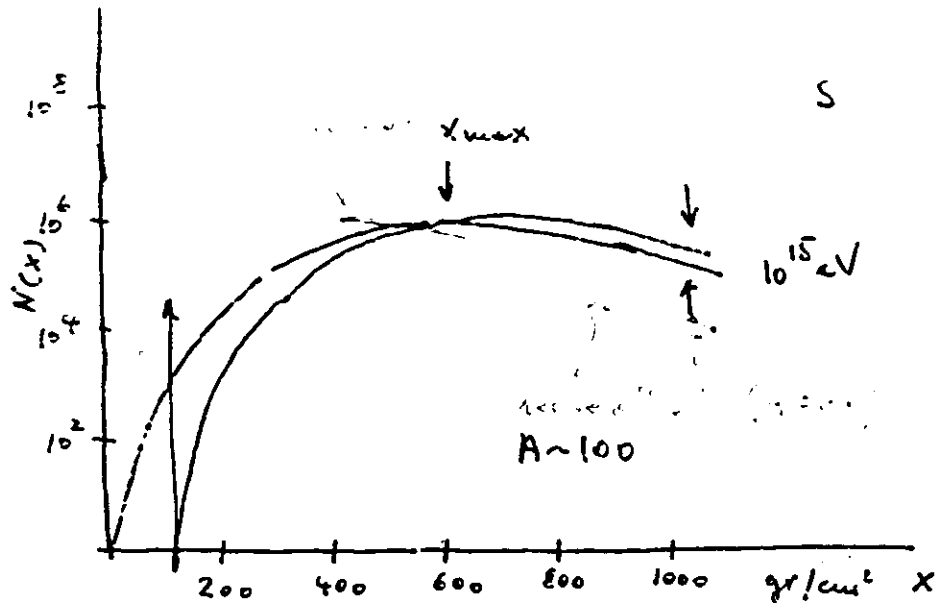

E_0

lateral spread of e.m. component

$\rho_e(\vec{r}) \rightarrow x_c, y_c \qquad \Delta T_i \rightarrow \vartheta, \vec{\Phi}$

$$\rho_e(r) = c(s)\,\frac{N_e}{r_0^2}\left(\frac{r}{r_0}\right)^{s-2}\left(1+\frac{r}{r_0}\right)^{s-4.5} \qquad \text{(Greisen 1956)}$$

$$N_e = \int_0^{\infty} 2\pi r\,\rho(r)\,dr$$

$N_e \rightarrow E_0$ simulations

non pure e.m. showers $\frac{E_{\mu vh}}{E_0} \sim 30\%$

$$E_{\mu vh} = \left(18^{+3.5}_{-1.5}\ \text{GeV}\right)\cdot N_\mu\,(>1\,\text{GeV})_{s.l.} \qquad \text{(Linsley 1983)}$$

non calorimetric (primary? x_{int}?)

$$Q_{C.F.} \simeq \int_0^{o.l.} e(x)\,N_e(x)\,dx \simeq E_{e.m.}$$

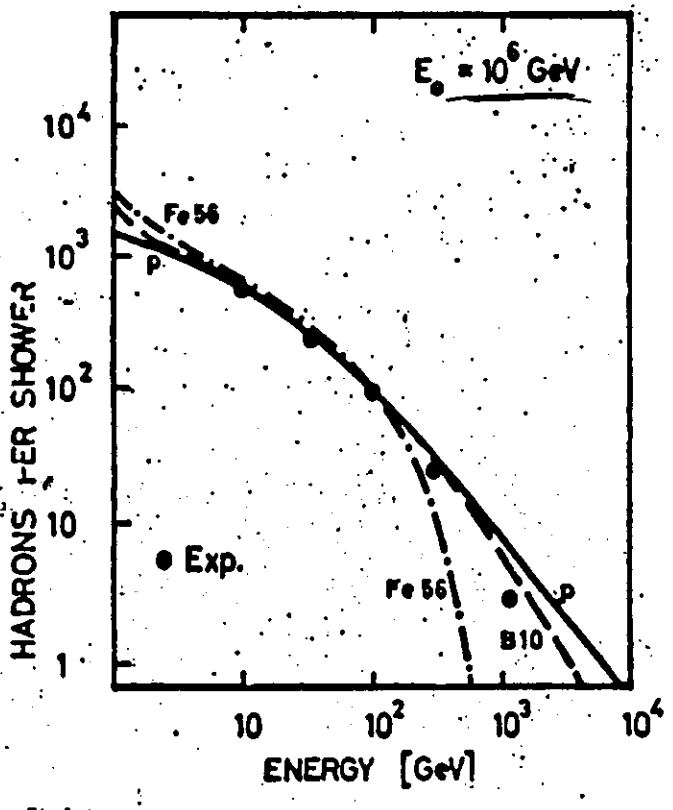

Fig.7 Average number and energy spectra of hadrons at mountain altitude (2000 m a.s.l.)for primaries of fixed energy and different mass (deduced from P.K.F. Grieder).
The distributions for E_0 100GeV are rather sensitive to the primary composition.

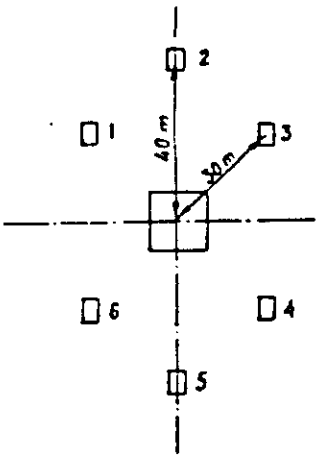

Arrangement of the array

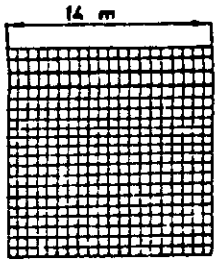

Central array

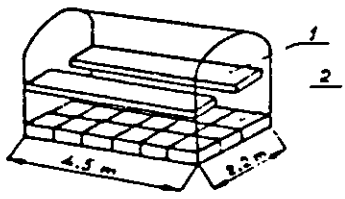

Outward detector

1 - G - M counters , 2 - scintillators

EA 3.1-6

TIEN SHAN

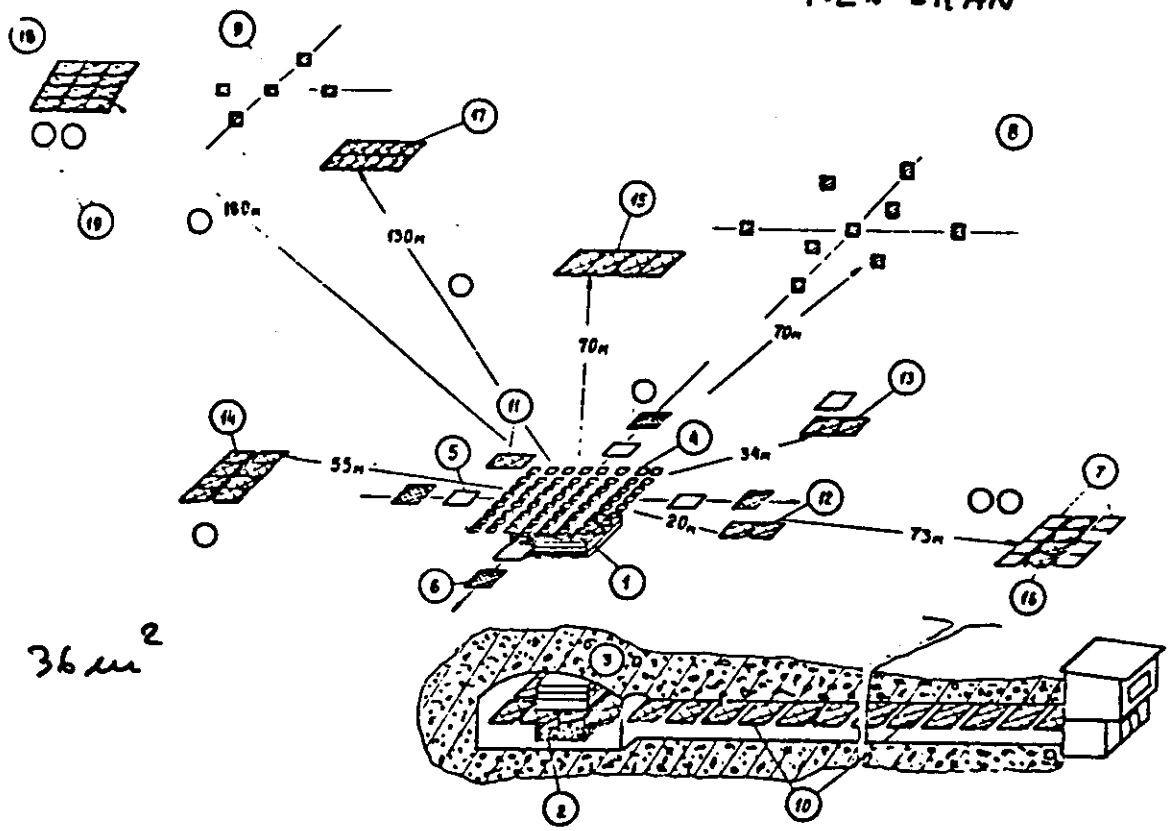

3800

Pb 36м²

fig.1

3. RESULTS AND DISCUSSIONS

The obtained experimental results about the lateral electron distribution in near vertical showers ($\theta < 30^0$) with constant sizes: A - Ne = (1.8-3.2).10^5; B - Ne = = (1.0-1.8).10^6 cannot be described by means of the NKG

HAVERAH PARK

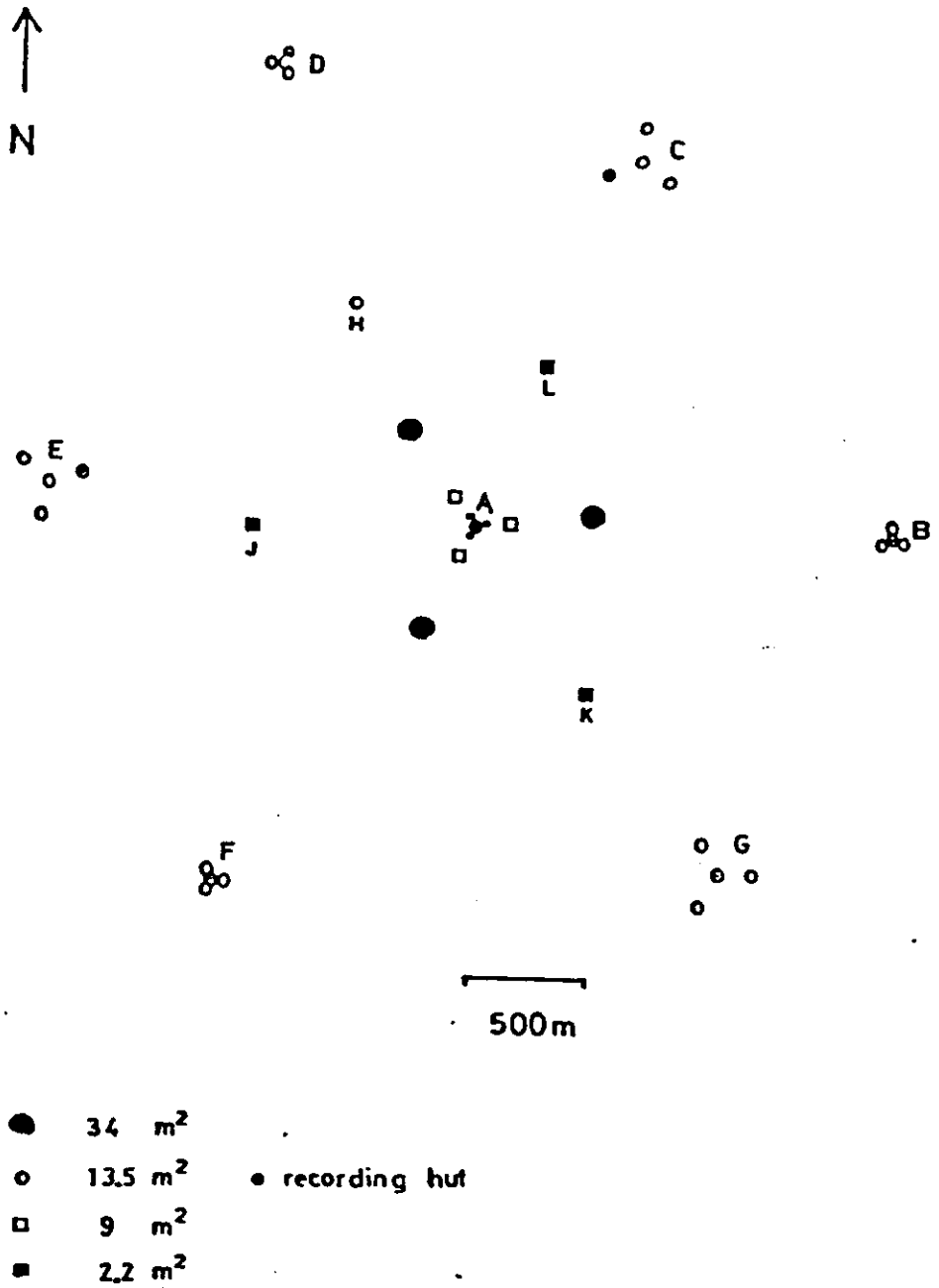

Fig. 2.1 Map of Haverah Park Array

AKENO

FIG.1 Tentative Arrangement

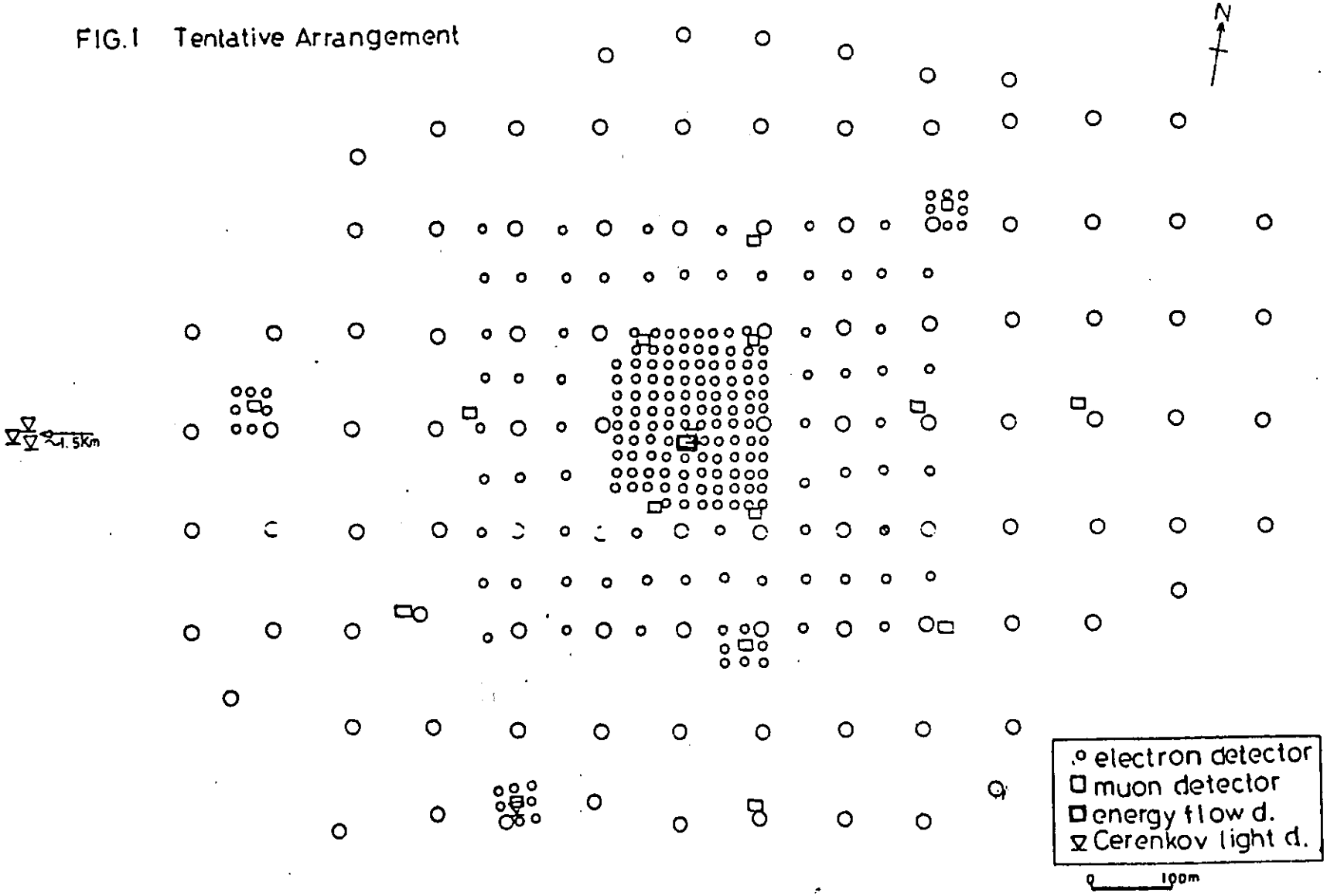

cascade curves for intensities: 10^{-10}, 10^{-11}, 10^{-} $cm^{-2}sec^{-1}ster^{-1}$ are in contradiction with the new Chacaltoya results [4] and in appropriate agreement with their old data [5] and MSU results.

The primary energy spectrum was reconstnucted on the base of the experimental obtained primary mass composition and their change with the energy [6] and traditional models of the hadron interaction. By the spectra recalculation was taken into account the body angle dependence of the muon number and shower size. The from the electron size and muon number spectra evoluted correspondent primary energy spectra $F_e(>E_o)$ and $F_\mu(>E_o)$ are in very good form agreement and the absolut intensity relation by $E_o = 10^{15}$ eV is $[F_e(>E_o)/F_\mu(>E_o)] \leq 1.2$. The obtained primary energy spectrum (fig.3) in good agreement with the ballon and satelite experiments [7] (shaded area) and Hillas (A)

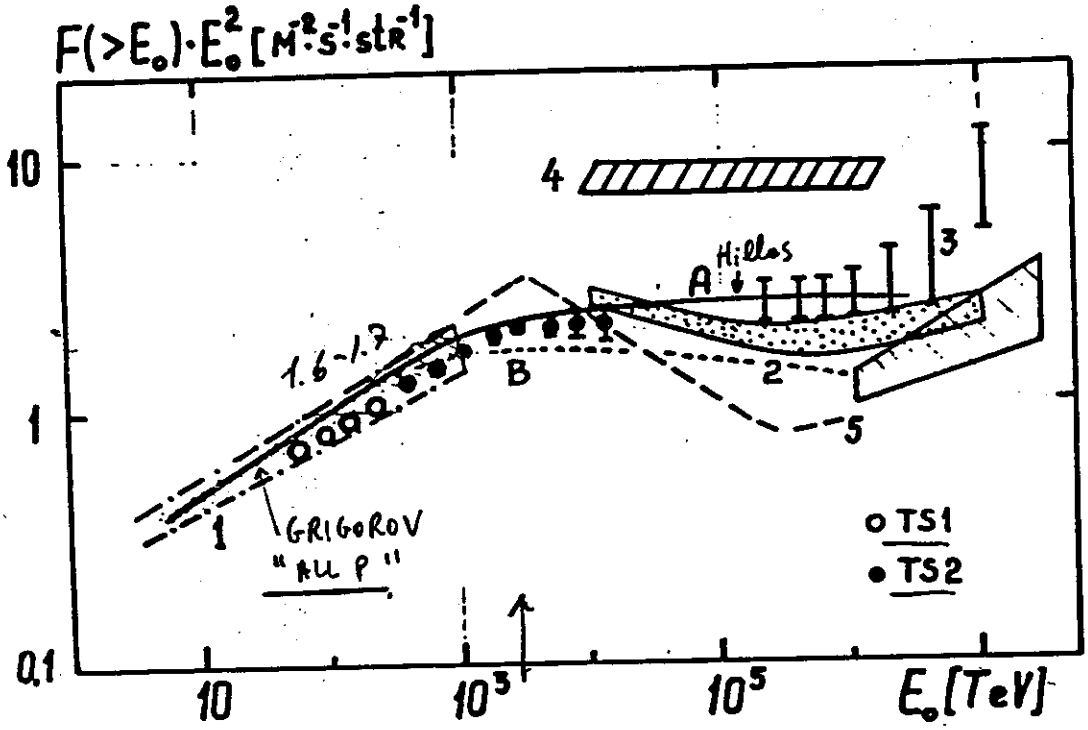

fig.3

primary spectrum prediction [8] and in contradiction with the Chacaltaya results [4]. The extrapolation of our $F(>E_o)$ spectrum is in good agreement with the Haverah Park [9] and Yakutsk [10] results.

I.N. KIROV et.al TIEN-SHAN
Proc. 17th ICRC, 2, 109 (1981)

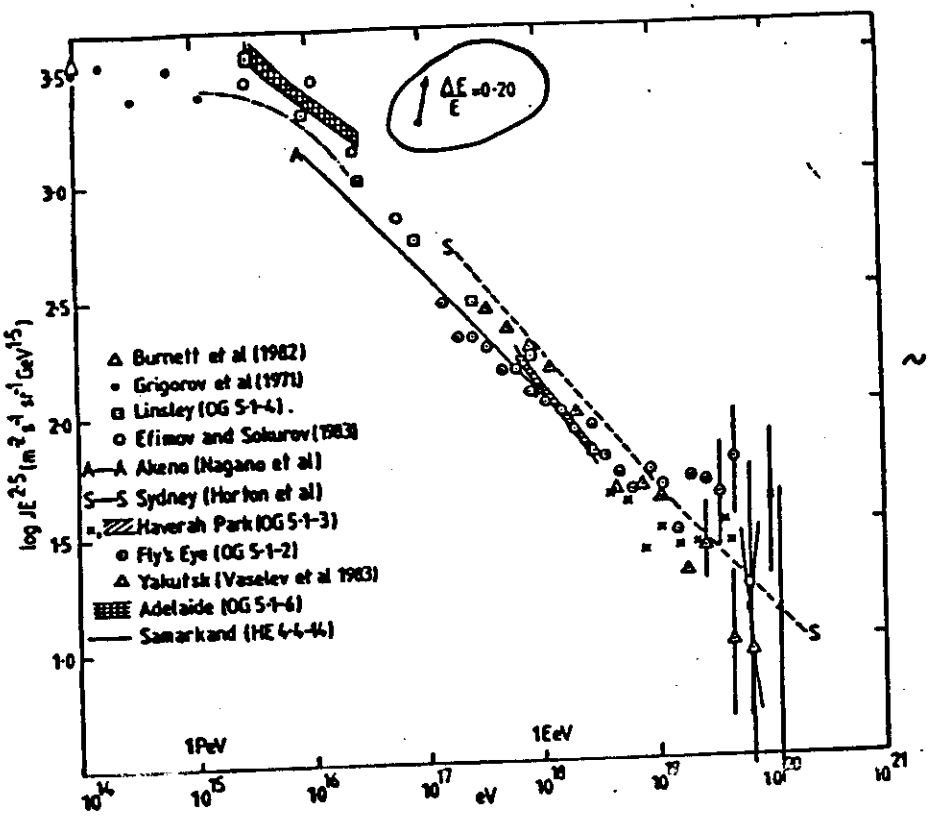

$\sim E^{-3.06}$

Figure 13: The differential energy spectrum from $10^{14} - 10^{20}$ eV. No attempt has been made to normalise data from different experiments. A systematic change in the energy assignment of 20% would shift each point as shown by the arrow; such a systematic effect could well be present in any data set and probably accounts for much of the scatter.

Table 3

Array	Exposure (km^2 y sr)	Events $>10^{20}$ eV
Volcano Ranch	~100	1
Haverah Park (OG 5.1-3)	320 ($\theta < 45°$)	4
	660 (used for anisotropy)	8
Yakutsk (OG 5.1-17)	200	0
Sydney (Horton et al 1985a)	1000	8
Fly's Eye (Baltrusaitis et al 1985a)	145	0
	Total	17

$$\frac{dN}{dE} = 1.6\,10^{7}\,E^{-3.06}\ m^{-2}\,sr^{-1}\,s^{-1}\,eV^{-1}$$

GREISEN - ZATSEPIN

$p + \gamma_{2.7°k} \rightarrow p + \pi^{\pm}_{0}$

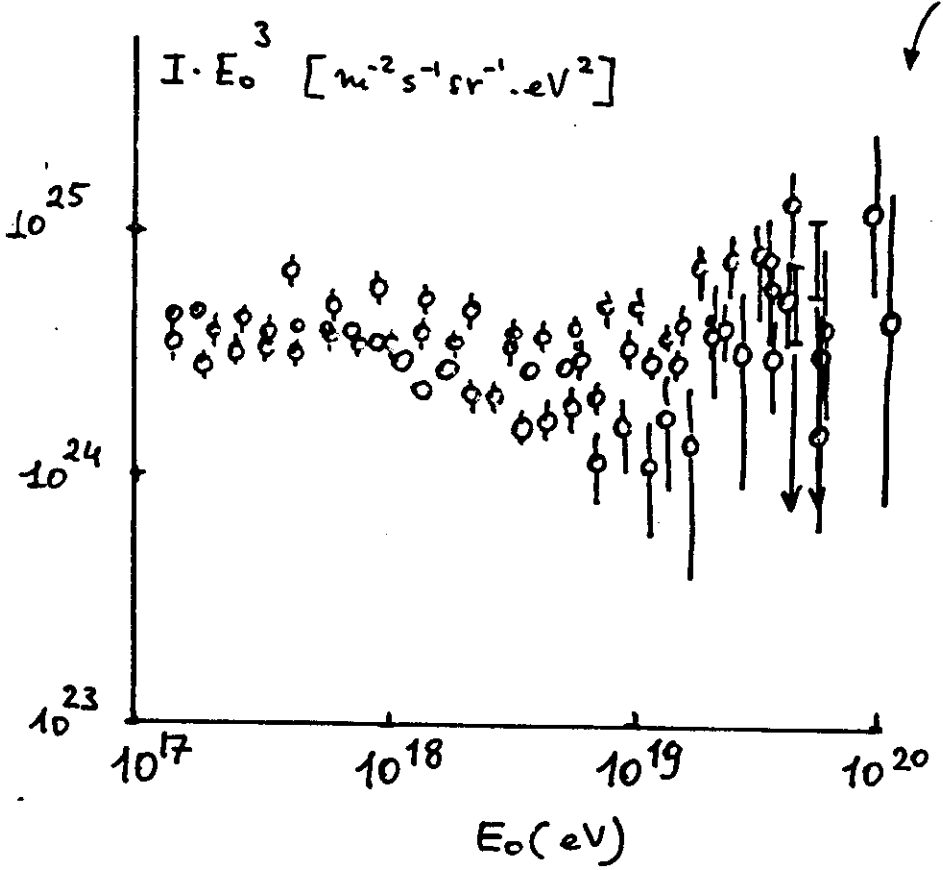

- HAVERAH PARK — 12 Km^2 WATER CER. DET.
  $\gamma\,(10^{18}eV) = 3.15 \pm 0.23$
  G. Brooke et al, Proc 19th ICRC, 2, 150 (1985)
- FLY'S EYE — ATH. FLORESCENCE LIGHT — $\sim 10^3 Km^2$ ($E_0 \sim 10^{20} eV$)
  $\gamma\,(< 10^{19}eV) = 2.94 \pm 0.02$
  $\gamma\,(> 10^{19}eV) = 2.42 \pm 0.27$
  R.M. Baltrusaitis et al, Proc 19th ICRC, 2, 146 (1985)
- AKENO — SCINT. — 20 Km^2
  $\gamma\,(< 10^{18}eV) = 3.02$
  $\gamma\,(10^{18} < E_0 < 10^{19} eV) = 3.39 \pm 0.06$
  $\gamma\,(> 10^{19}eV) = 2.0 \pm 0.2$
  M. Teshima et al, Proc. 20th ICRC, 1, 404 (1987)
- YAKUTSK — SCINT + ATH. C.L. — 20 Km^2
  $\gamma\,(\sim 10^{18.5}) = 3.63 \pm 0.05$
  $\gamma\,(\sim 10^{19}) = 2.47 \pm 0.09$ $\quad \gamma\,(> 10^{19.5}) = 3.48 \pm 0.11$
  D.D. Krasilnikov et al Proc 19th ICRC, 2, 190 (1985)
  G.B. Khristiansen Proc. 19th ICRC, 9, 487 (1985)

SYDNEY μ. det ~80km²

Bell et al J. Phy A Nucl Gen, 7, 990 (1974)

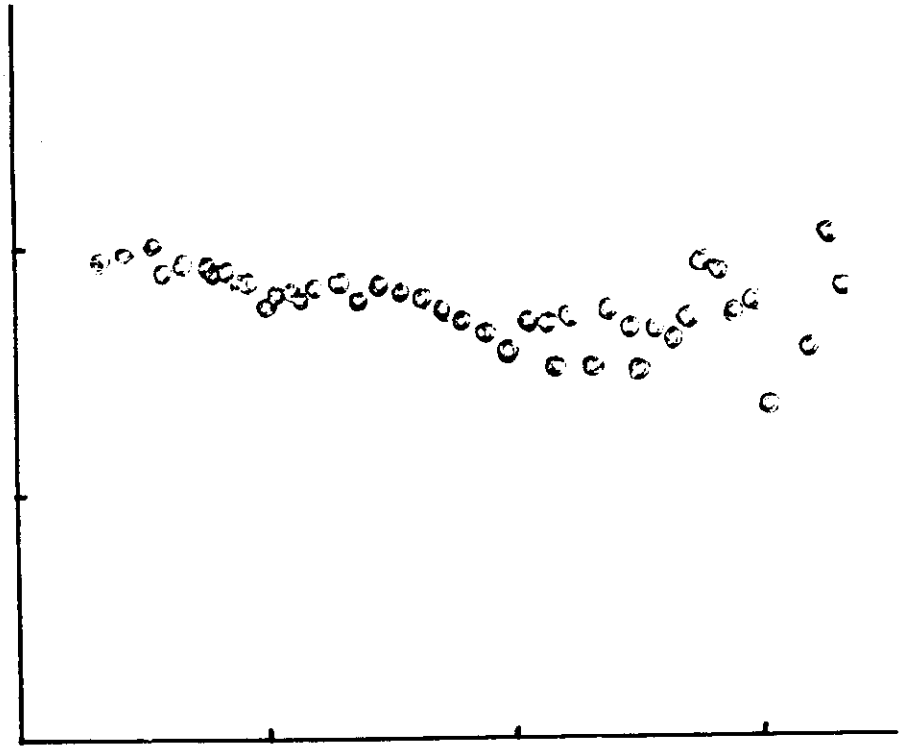

$$f(m) = \Sigma_A \int_{E_{th}} P(m, N_\mu) \cdot S_A E_0^{\gamma_A} dE_0$$

$$\bar{N}_\mu = .0145 \frac{A}{E_\mu} \left(\frac{E_0}{A E_\mu}\right)^{.757} \left(1 - \frac{A E_\mu}{E_0}\right)^{5.25} \quad \text{(Elbert + Gaisser)}$$

387

The Baksan group has used two methods to derive the composition. The first one is similar to the approaches of the two other groups [HE 5.5-12]. Figure 4 shows the multiplicity distribution in the detector compared with predictions for pure compositions of different A (solid lines) and two composition models. A light energy-independent composition with $\langle A \rangle = 3.5$ best fits the data. $\langle A \rangle = \sum \beta_i A_i^2 / \sum \beta_i A_i$, where β_i is the fraction of nuclei with mass A_i on *E/nucleon* basis.

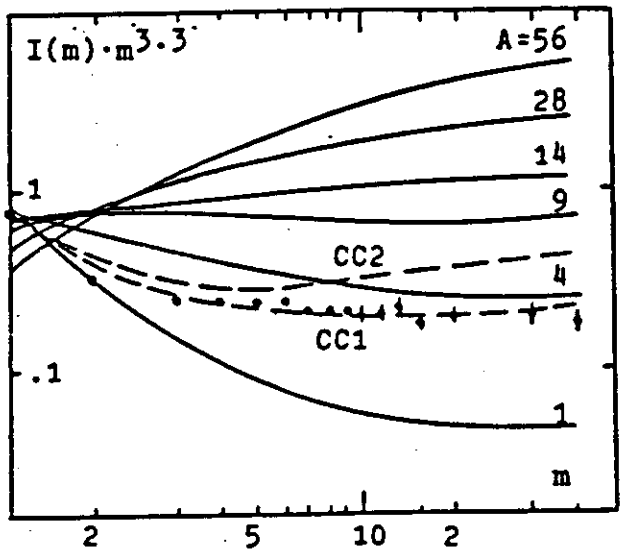

E.V. Budko et al
Proc. 19th ICRC
8, 24 (1985)

Fig. 4. Comparison of Baksan multiplicity distribution with predictions from pure (solid lines) and mixed compositions.

Note that because of the relatively shallow and large detector ($E_\mu > 0.22$ TeV) the observed multiplicities reach very high values.

The second approach is more interesting, because it involves an estimate of the primary energy [HE 5.1-13]. It is based on a calculated relation of the energy of the muon-induced showers in the detector to the primary energy per nucleon, which fits some other properties of the detected muon groups.

Figure 5 shows the observed dependence of the muon multiplicity N_μ on the primary energy E_0/A estimated through the energy of muon-induced showers in the detector. Curve 2 corresponds to a composition with $\langle A \rangle = 3.5$ and curve 3, which seems to fit data quite well, has $\langle A \rangle = 4.5$.

The conclusion from both approaches is that the primary composition does not change with energy and is dominated by protons up to 10^{15} eV.

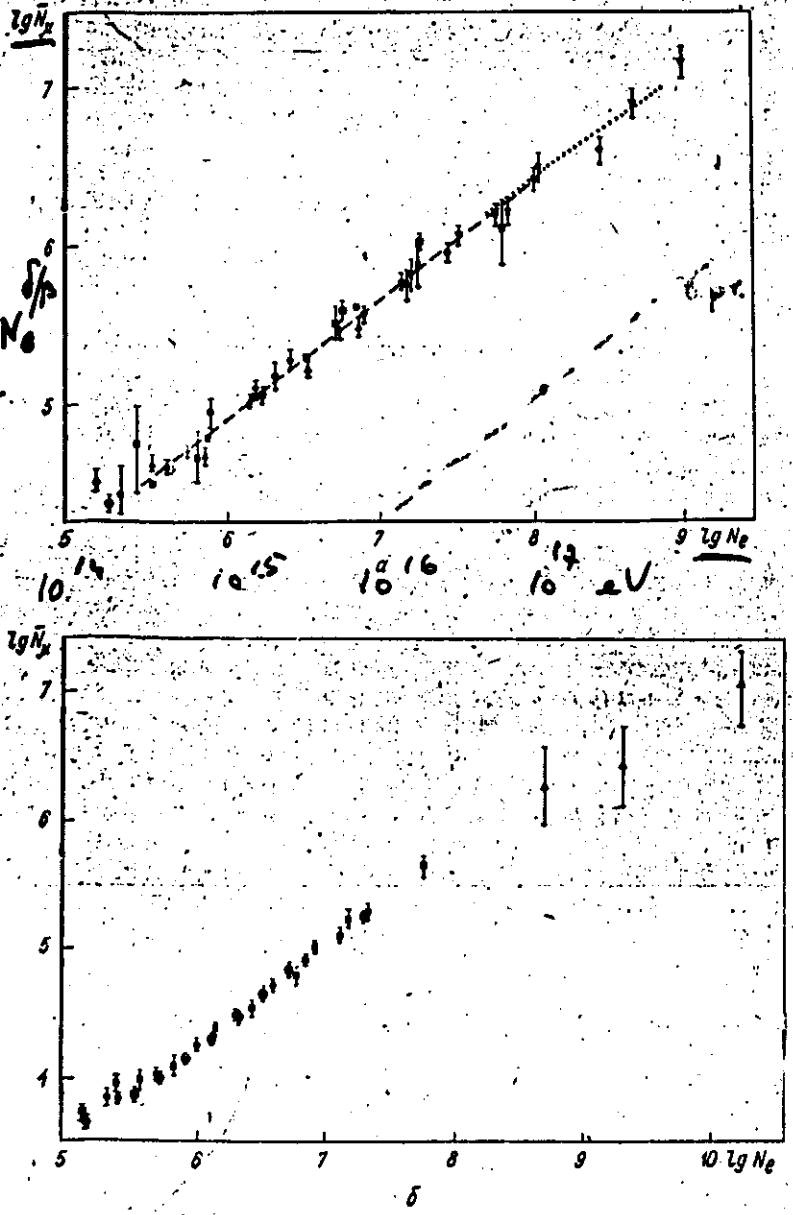

Рис. 4.33. Зависимость среднего числа мюонов различных энергий от числа частиц в ливне при $E_\mu > 1$ *Гэв* (*а*) и $2 < E_\mu < 10$ *Гэв* (*б*):
а: ▼—[271] (x=800 *г/см²*); ■—[185] (уровень моря); ⊕—[204] (x=500 *г/см²*); . . . —[203] (x=500 *г/см²*); ■—[289] (x=700 *г/см²*); ▲—[181] (x=800 *г/см²*); — — — —[142] (уровень моря); ●—[198] (уровень моря); ○—[107] (уровень моря);
б: ⊕—[322] ($E > 2$ *Гэв*); ●—[342] ($E > 10$ *Гэв*); ▲—[252] ($E > 5$ *Гэв*); ■—[273] ($E > 5$ *Гэв*)

if the composition is the same as at low energies. This suggests that heavy primaries are absent at energies above 10^{17} eV per nucleon. Its significance will be discussed in Chapter 6.

The existence of γ-primaries may be seen from the existence of *few muon events*. The distribution of N_μ/N for $5 \times 10^5 < N < 5 \times 10^6$ observed at distances from the axis greater than 25 meters at Mount Chacaltaya is similar to that in Fig. 5.29, but at the smallest part we find a peak, as shown in Fig. 5.31*a*. The frequency of such showers is 5×10^{-4} of the total frequency of EAS of the same size. At larger sizes, $N \geq 5 \times 10^6$, the peak is not seen, as shown in Fig. 5.31*b*.

Whether or not the low muon peak belongs to a different kind of EAS may be determined by observing the zenith-angle distribution, which

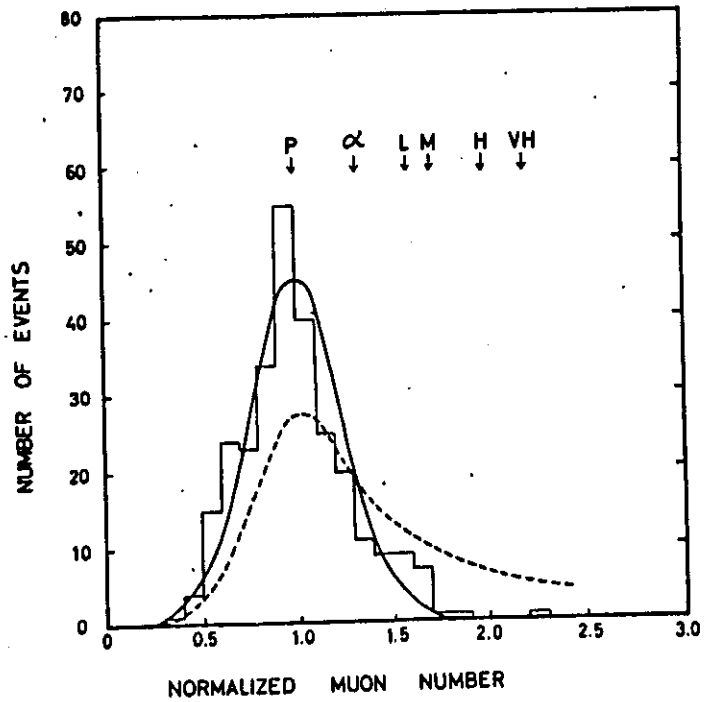

Fig. 5.30 The distribution of muon size (Toyoda 65). Data are taken from 280 EAS with $N \geq 5 \times 10^7$. The solid curve represents a Gaussian distribution, expected if primary particles consist of protons alone. The dashed curve represents a distribution expected if the composition of primary cosmic rays is the same as at low energies; p, α, etc., and arrows indicate the positions of peaks of the N_μ-distributions due to the various primary particles.

jev et al.(EA4-1) have added Cerenkov detectors to their AS
are placed at distances from 30 to 245 m from the center
the lateral distribution of Cerenkov photons(LDC). The
re of Cerenkov light at 200 - 300 m was measured by
al.(EA4-6) by 7 photomultipliers(PM) with a conical mirror
:a 1240 cm^2. Showers with zenith angles less than 35^o were
'he time resolution is 11 ns (FWHM). The pulse widths
) - 260 m are normalized to tw(200m) according to
Since their observation level is too near the shower
g/cm^2), their result may be a lower limit for t(max) and
s plotted
an arrow.

erenkov
sts of

or LDC
pulse
ter for
...e
(Kalmykov
2). The
riggered
nkov
and the
rgy can
ied from
good
ir each
ie LDC

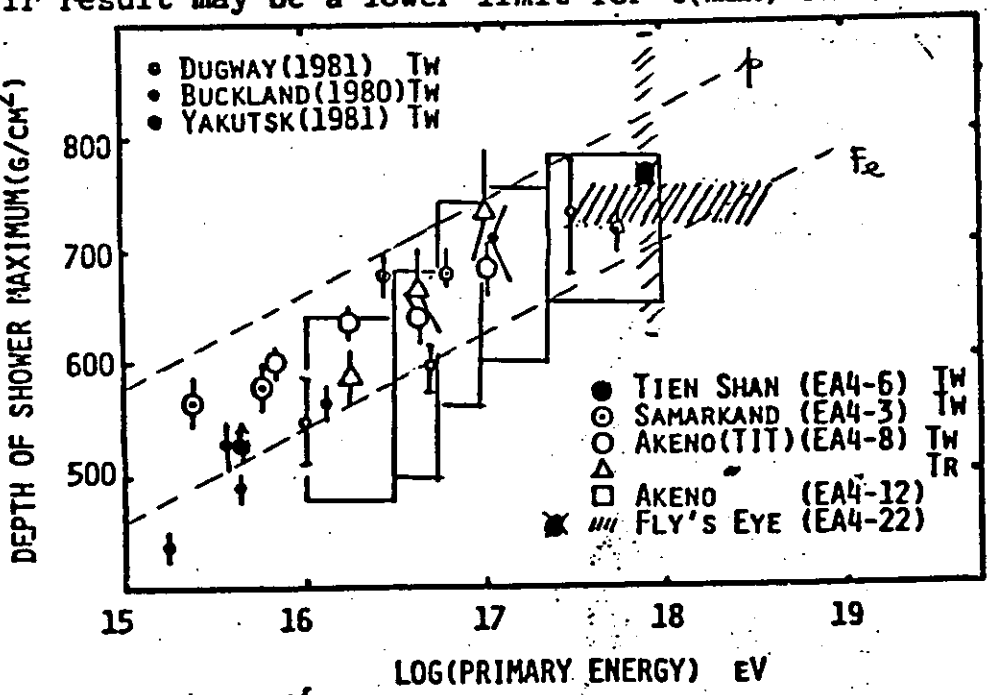

Fig.2 Summary of measurements of t(max) at this conference. Some earlier work based on tw are also plotted as small symbols.

H. Nagano Rep. Prog. Phys. Bangalore (83)

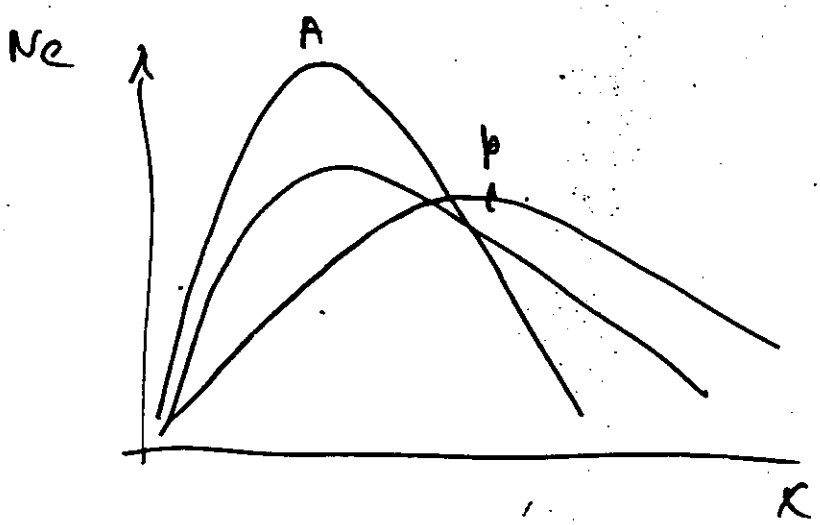

$$X_M = \frac{W_0}{\epsilon_c}$$

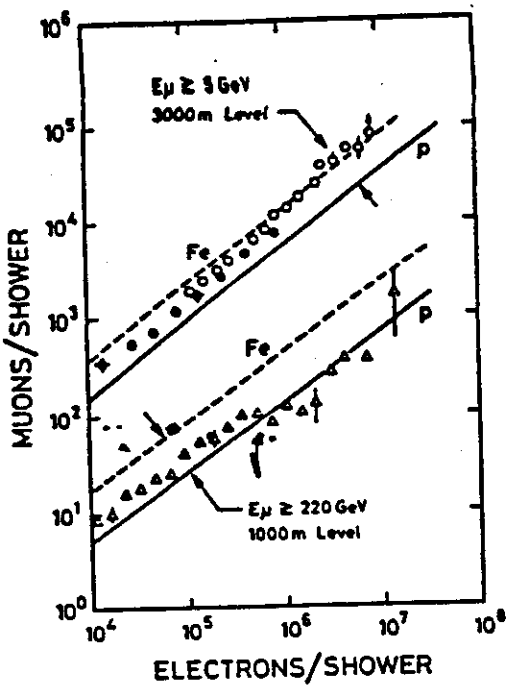

P.K.F. GRIEDER
Proc 19th ICRC, 2, 214 (1985)

Fig. 2 Muon - electron correlations for proton and iron initiated showers. The dashed and solid lines are from our calculations. The full and open circels are experimental data from Tien Shan (Kabanova et al., 1973 and Machavariani et al., 1979), the triangular symbols from the Kolar Gold Fields (Acharya et al., 1983). Proc 18th ICRC, 9, 191 (1983)

...ack of space does not allow us to summarize the hadron data